Thin-film magneto-inductive cables

R R A Syms, L Solymar, I R Young, T Floume

Thin-film Magneto-Inductive Cables

by

R.R.A.Syms*, L.Solymar, I.R.Young and T.Floume

Abstract

Magneto-inductive cables for low (ca 100 MHz) radio frequencies are demonstrated in thin-film form. 20 cm long resonant elements are formed using double-sided patterning of copper-clad polyimide, based on single-turn inductors and parallel plate capacitors that use the substrate as an interlayer dielectric. Continuous cables are formed by overlaying elements, in an arrangement that allows a high, positive coupling coefficient ($\kappa > 0.6$) to be achieved despite the use of a planar geometry. Equivalent circuit parameters are extracted from experiments on integrated coupling transducers, and propagation characteristics are compared with simple theory. Low propagation loss (4 dB/m at 55 MHz, falling to 2.3 dB/m at 130 MHz) is demonstrated near the operating frequencies of magnetic resonance imaging, for a potential application as patient-safe cable in internal imaging.

KEYWORDS Metamaterial, periodic structure, magneto-inductive wave

PACS numbers 41.20.-q Applied classical electromagnetism

81.05.Zx New materials: theory, design and fabrication

84.30.Bv Circuit theory

Optical and Semiconductor Devices Group, EEE Dept., Imperial College London, Exhibition Road, London SW7 2AZ, UK

*Corresponding Author: TEL +44-207-594-6203 FAX +44-207-594-6308 Email r.syms@imperial.ac.uk

1. Introduction

Recently there has been considerable interest in artificial electromagnetic structures that may have novel properties such as negative permittivity, permeability and refractive index [1-3]. Many are based on periodic arrays of resonant elements, and are therefore similar to those historically used in filters and slow wave circuits [4, 5]. However, wide-ranging research has extended the range of applications and operating frequencies very considerably [6-8].

One example of a simple metamaterial is the magneto-inductive (MI) waveguide [9], sometimes called a metasolenoid [10, 11]. The resonant element is a simple L-C circuit, which is magnetically coupled to its neighbours by a mutual inductance M as shown in Figure 1a. There are two main variants: the axial (Figure 1b) and planar (Figure 1c) configurations, in which M is positive and negative, respectively. MI waves have been studied extensively, in one-dimensional (1D) waveguides [12-15] and in 2D and 3D arrays [16, 17]. Applications have been identified in magnetic field concentration [18], delay-lines [19], phase shifters [20], filters and splitters [21] and near-field lenses [22, 23].

A recent application is patient safety during *in-vivo* internal magnetic resonance imaging (MRI) [24, 25], a generalisation of earlier work in which co-axial cables carrying the signal from catheter-mounted detectors were subdivided using thin-film transformers [26]. Here, division into lengths shorter than the resonant length for external excitation

prevents heating by the electric field of the powerful RF transmitter [27, 28]. The critical length is $c/(2f\sqrt{\varepsilon_r})$, where c is the velocity of light, f is the frequency and ε_r is the relative dielectric constant of any surrounding tissue. For ^{1}H MRI in a 1.5 T field, f = 63.8 MHz, ε_r = 77 for human tissue and the critical length is around 27 cm.

Previously, MI waveguides have been constructed as discrete elements based on wire-wound [12] or printed circuit board [14] inductors and surface mount capacitors. However, construction has involved tedious assembly and tuning, and propagation losses have been extremely high. Taking into account the element spacing, published attenuation figures of ≈1.5 dB/El in [12] and ≈ 0.12 dB/El in [14] translate into propagation losses of ≈150 dB/m and ≈ 50 dB/m, respectively. These high values rule out most practical applications.

A key requirement is therefore low-cost fabrication of high-performance material, especially in long lengths, large areas or flexible formats. Metamaterials such as dipoles, Jerusalem crosses, wire pairs and split-ring resonators are now being fabricated using single-sided patterning of metal layers on flexible dielectric substrates [29-35]. This approach has been successful at terahertz frequencies, when only small effective component values are required and sufficient capacitance can be obtained using a coplanar geometry [32-35]. However, for a MI waveguide operating at MHz frequencies, large values of L and C are required.

In this paper, a novel resonant element that allows low-loss, low frequency magneto-inductive waveguides to be formed as continuous thin-film cables is introduced. Double-sided patterning of flexible copper-clad polyimide is used to form elements that combine loop inductors with integrated parallel-plate capacitors, and low-loss propagation is demonstrated at MRI frequencies over the two-metre lengths typical of catheter-based internal imaging probes. We believe these to represent the longest continuous metamaterial structures demonstrated to date. The approach also allows the incorporation of integrated coupling transducers. The design is introduced in Section 2, fabrication and experimental characterisation are described in Section 3, experimental results are compared with the predictions of simple theory in Section 4 and conclusions are presented in Section 5.

2. Design

We first briefly review the underlying theory of magneto-inductive waveguides [9]. Applying Kirchhoff's laws to the n^{th} loop in Figure 1a, we obtain:

$$\{j\omega L + 1/j\omega C + R\}I_n + j\omega M\{I_{n-1} + I_{n+1}\} = 0 \quad (1)$$

Here $\omega = 2\pi f$ is the angular frequency and f is the corresponding temporal frequency. Here we have introduced resistors R to denote lossy inductors. Assuming that the currents I_n may be taken in the form of a travelling wave as $I_n = I_0 \exp(-jnka)$, where ka is the phase shift per element, k is the propagation constant and a is the period, the dispersion equation may be obtained as:

$$\{1 - \omega_0^2/\omega^2 - j/Q\} + \kappa \cos(ka) = 0 \quad (2)$$

Here $\omega_0 = 2\pi f_0 = 1/\sqrt{(LC)}$ is the angular resonant frequency, f_0 is the corresponding temporal frequency, $Q = \omega L/R$ is the Q-factor, and $\kappa = 2M/L$ is the coupling coefficient. Assuming that $k = k' - jk''$, and losses are small, Equation 2 may be approximated as:

$$(1 - \omega_0^2/\omega^2) + \kappa \cos(k'a) = 0$$

$$k''a = 1/\{\kappa Q \sin(k'a)\} \quad (3)$$

The upper equation in (3) is the dispersion relation for loss-less waves. In the axial

configuration, κ is positive, the waveguide supports forward waves and propagation is obtained only over the frequency band $1/(1 + \kappa) \leq (\omega/\omega_0)^2 \leq 1/(1 - \kappa)$, whose extent depends on the value of κ. The lower equation shows that losses are lowest at mid-band ($k'a \approx \pi/2$) and are reduced by a high Q-factor and a large coupling coefficient. In the planar configuration, κ is negative and backward waves are supported.

From the point of view of propagation loss, neither configuration is entirely satisfactory, since it is more often loss per metre that is important than loss per element. Planar elements can have a large physical extent in the direction of propagation, but have a relatively small coupling coefficient since $|\kappa| < 1$ in this geometry. Experimental values are usually lower. Axial elements have a larger coupling coefficient, with a peak value that can approach $\kappa = 2$, but only if the period is so small that the distance propagated per element is extremely short.

We therefore introduce the modification shown in Figure 2a (which omits resistive losses) in which the capacitor and inductor are each separated into two series-connected elements. This new arrangement has the same dispersion relation as that of Figure 1a. However, sub-division of the inductor allows adjacent resonators to be overlaid so that large, positive coupling is achieved in a planar geometry, as shown in Figure 2b. Sub-division of the capacitor allows the formation of high-value integrated parallel plate components that use a thin substrate as a dielectric interlayer as shown in Figure 2c. Both sides of the substrate carry inductor loops and capacitor plates and a cable is realised by cascading sections so that inductors from adjacent elements overlay to form air-cored

transformers.

In addition to reducing loss and improving manufacturability, this arrangement should reduce the relative size of non-nearest neighbour coupling, a feature that has complicated understanding and development of magneto-inductive devices [15]. However, departures from ideal behaviour are still likely to arise from parasitic capacitances C_1 between the tracks of overlapping inductors and C_2 between the plates of adjacent capacitors. Careful choice of design dimensions is required to minimise their effect.

Cable layouts are specified using the parameters of Figure 3a, which shows one period. Elements are defined in terms of their overall width W and half-length D_P (= a). Inductors are defined in terms of their half-length D_L and track width T. Capacitor plates are defined in terms of their half-length $D_C = (D_P - D_L)/2$, and a gap G_C between the plates is used to reduce C_1. A gap G_L is used to separate the inductors and capacitors, and a further transverse separation S_L is introduced between the tracks on either side of the substrate to reduce C_2. Periodic repetition allows a complete cable to be defined, together with inductors that can act as integrated transducers for input and output coupling as shown in Figure 3b. The overall length of a cable with N resonant elements is then $(N + 1)D_P$.

3. Fabrication and experimental characterisation

Prototype thin film MI cables were fabricated in two metre lengths by the UK company Clarydon (Willenhall, West Midlands), using double-sided patterning of copper-clad polyimide. The starting material was 25 μm thick Kapton® HN (DuPont, Circleville, OH), coated on each side with a 35 μm thick pressure-bonded layer of copper. The copper was patterned by lithography and wet chemical etching, using two consecutive exposures to a pair of one-metre-long photomasks whose layouts were defined by a Gerber file. Registration to the Kapton sheet was achieved using mechanical alignment pins.

Dimensions for operation at MRI frequencies were estimated from earlier work. PCBs were fabricated as panels measuring 300 mm x 2 m. Each panel contained three repeats of an array containing eight different MI cables with the parameters given in Table I. In each case, the same value of D_P = 10 cm was used, so that the overall element length of 20 cm was less than the critical value given earlier. A 2 m long panel then contained 200/10 - 1 = 19 resonant elements. The overall width W was taken as 4.7 mm throughout, to place the conductors on the diameter of an 8 Fr (2.7 mm dia) catheter. The lengths D_L and D_C of the inductors and capacitors were varied across the array to obtain a variation in the resonant frequency f_0. The widths of all narrow features including track widths and clearance gaps (T, G_C, G_L, and S_L) were taken as 0.5 mm, the minimum feature size that could be patterned reliably over a 2 metre length. Figure 3c shows a completed array with design A at the top and H at the bottom, from which individual guides can be separated using a scalpel.

Electrical performance was measured using an Agilent E5061A Electronic Network Analyser. The equivalent circuit parameters are given in Table I and were extracted from measurements of integrated transducers. A large capacitor C_T = 1 nF was first soldered across a transducer, which effectively comprised half an element, to create a new element defined mainly by L/2 and C_T. The resonant frequency f_{T1} of this element was found by inductive probing, and used to estimate L. The capacitor was then removed, and a short circuit soldered across the two half-length capacitor plates at the substrate rear below the transducer connections, to create a further new resonant element now defined mainly by L/2 and C/2. The resonant frequency $f_{T2} = f_0/2$ of this element was then used to estimate C. Component values extracted from either end of the same cable were consistent, suggesting good dimensional control. Figure 4a shows the variation of L and C with D_L; both vary linearly to good approximation. Figure 4b shows the corresponding variation of f_0, which shows that the designs straddle the frequency range from 63.8 MHz to 127.6 MHz, corresponding to ^{1}H MRI at fields between 1.5 T and 3 T.

The extracted capacitance may be compared with an estimate $C_{est} = D_C(W - G_C)\varepsilon_0\varepsilon_r/2t$ obtained from a parallel plate model, where $\varepsilon_0 = 8.85 \times 10^{-12}$ F/m, and $\varepsilon_r = 3.5$ is now the relative dielectric constant and t = 25 μm is the thickness of the polyimide sheet. The extracted values are generally smaller than these estimates, suggesting experimental error in the determination of f_{T2} (and hence also in f_0) caused by proximity to the propagating band.

Cable properties were determined after attaching SMA connectors to the input and output transducers and connecting to the network analyser. The cables could be flexed gently without significant variations in transmission. However, folding the cables so resonators at different points could couple magnetically did introduce changes. Figure 5 shows the frequency variation of the S-parameters of two-metre lengths of four different cables (A, D, F and G). The remaining designs have equivalent performance at appropriate frequencies.

Figure 5a shows the frequency variation of S_{21}. In each case, propagation is band-limited, with the centre frequency and bandwidth increasing from Design A to G. Out of band, there is increasing transmission at higher frequencies, which is attributed to the parasitic capacitance C_1 in the transformers. Overall transmission also increases from design to design, but relatively slowly. For Design A, for example, propagation is obtained from 44 MHz to 88 MHz, and minimum insertion loss of around 11 dB is obtained near 63.8 MHz frequency. For Design G, minimum loss has reduced to around 7.5 dB, and, this design would be suitable for operation at 127.6 MHz. Figure 5b shows the frequency variation of S_{11}. In each case, impedance matching is moderate, with a minimum return of around -5 dB for Design A reducing to -7 dB for Design G. These results suggest that the majority of the insertion loss must be due to attenuation rather than coupling loss.

After measurement, lines were attached to the outside of 8 Fr catheters using heat-shrink tubing, and re-measured. The only change in performance was a slight increase in centre

frequency following from the reduction in inductance L caused by the change in geometry.

4. Comparison with theory

To compare the experimental results with theory, a method of estimating S-parameters is required. We use a simple approach that ignores multiple reflections, but which also neglects loss in calculation of reflection coefficients and hence is valid only for intermediate attenuation. To estimate reflection losses, we assume the geometry of Figure 6a, where a semi-infinite line ending at element 0 is terminated using a resistor R_L via an inductive transducer. Other resistive losses are ignored. For the final elements, Kirchhoff's laws give:

$$\{j\omega L + 1/j\omega C\}I_0 + j\omega M\{L_1 + I_L\} = 0$$

$$\{R_L + j\omega L/2\}I_L + j\omega M I_0 = 0 \qquad (4)$$

From the lower equation in (4) the load current can be found. Substituting into the upper equation, we obtain:

$$\{j\omega L + 1/j\omega C + Z_L\}I_0 + j\omega M L_1 = 0 \qquad (5)$$

Here $Z_L = \omega^2 M^2/\{R_L + j\omega L/2\}$ is an effective load impedance. A solution is now attempted as a sum of counter-propagating waves, i.e. as $I_n = I_I \exp(-jnka) + I_R \exp(+jnka)$ where I_I and I_R are incident and reflected wave amplitudes. This solution automatically satisfies the loss-less recurrence equations away from the termination. Substituting into

Equation 5, and using these relations, we can obtain the reflection coefficient $\Gamma = I_R/I_I$ for current waves as:

$$\Gamma = -\{Z_L - Z_0\}/\{Z_L + Z_0^*\} \tag{6}$$

Here Z_0 is the characteristic impedance of a MI waveguide, previously found in as [8]:

$$Z_0 = j\omega M \exp(-jka) \tag{7}$$

and Z_0^* is the complex conjugate of Z_0. At mid-band ($ka = \pi/2$), Z_0 is real and has the value $Z_{0M} = \omega_0 M$. In principle, it should be possible to match Z_{0M} to a real resistive load by appropriate choice of M and by making the effective termination Z_L real at f_0, using an additional series capacitor. In this case we simply require $\omega_0 M = R_L$.

Including propagation losses arising from the imaginary part of the propagation constant, but neglecting multiple reflections, the scattering parameters of an N-element waveguide with identical terminations at either end may then be expressed in dB as:

$$S_{11} \approx 10 \log_{10}\{|\Gamma|^2\}$$
$$S_{21} \approx 10 \log_{10}\{(1 - |\Gamma|^2) \exp(-2Nk''a) (1 - |\Gamma|^2)\} \tag{8}$$

Theoretical estimates obtained from Equations 3 and 6-8 were compared with experimental data as follows. The inductance L was assumed to be accurately determined.

The resonant frequency f_0' (an approximation to f_0 obtained by matching theory to experiment), Q-factor and coupling coefficient κ were then adjusted to fit the centre frequency, bandwidth and maximum transmission, respectively. Figure 6b shows a typical comparison between experiment and theory for the frequency variation of S-parameters of Designs A and G, assuming $R_L = 50\ \Omega$. Generally, the agreement is excellent, although the theory clearly cannot predict the oscillations arising from multiple reflections.

The fitting parameters are detailed in Table I, and the variation of f_0' with D_L is superimposed on Figure 4b for comparison with the earlier estimate. Discrepancies between f_0' and f_0 confirm the small inaccuracy in experimental determination of the latter. The Q-factor is modest, rising quasi-linearly with f_0' from 36 in Design A to 55 in Design H, as shown in Figure 7a. The coupling coefficient κ rises slowly with D_L from 0.61 to 0.69, suggesting that the central sections of the inductors provide slightly more effective coupling than the ends. The combination of rising Q-factor and coupling coefficient causes a reduction in propagation loss. At mid-band, the loss per element can be found in dB from Equation 3 as:

$$\text{Loss/El} = 10 \log_{10}\{\exp(-2/\kappa Q)\} \tag{9}$$

This value can be converted into an equivalent loss per metre by dividing by the repeat distance D_P (= a). Figure 7a also shows the variation of propagation loss with f_0'. The loss falls from ≈ 0.4 dB/element to ≈ 0.23 dB/element (or 4 dB/m to 2.3 dB/m) over the range shown. Compared with earlier MI waveguides [14], the second figure represents a

twenty-fold reduction in loss per metre, largely due to the increased size of the new elements.

Finally we show in Figure 7b the variation with the inductor length D_L of the mid-band impedance Z_{0M}. The impedance rises from ≈ 20 Ω in Design A to ≈ 70 Ω in H, due to a combination of a slow increase in M and a more rapid rise in f_0. Since the values are close to 50 Ω, it should be relatively simple to reduce coupling losses by small changes in layout.

5. Conclusions

Low-loss propagation of magneto-inductive waves has been demonstrated using thin-film cables fabricated entirely by double-sided patterning of copper-clad polyimide. The resonant elements are formed using single-turn inductors and parallel plate capacitors that use the substrate as a dielectric interlayer. Integrated coupling tranducers are also formed from single-turn inductors. Large, positive coupling between elements is obtained despite the use of a planar arrangement, and the availability of high-value integrated capacitors allows operation at low (100 MHz) frequencies. The fabrication method is intrinsically low-cost and extensible to long lengths using step-and-repeat patterning, and should allow rapid development of other thin-film magneto-inductive components such as splitters and filters. Low insertion and propagation losses have been demonstrated over two-metre lengths. Experimental measurements of S-parameter variations have been compared with the predictions of a simple theoretical model, and good agreement has been obtained. Further improvements in performance and a reduction in element size should follow from the use of multi-turn inductors. These aspects are now being investigated.

Finally we note that a time-varying external magnetic field can induce voltages in the open loops. However, if the external field is slowly varying in space, the overall voltage can be minimised by replacing open loops with figure-of-eight windings, so that induced voltages in each half-winding at least partly cancel. This arrangement would avoid RF heating or damage by the transmit field in a MRI scanner, together with any substantial

modification to the excitation pattern [36]. Voltages induced by faster-varying fields from local dipole distributions would not necessarily be subject to such cancellation. However, any resulting signals would be encoded in frequency space by the gradient fields, and could be separated out by scanner software. Such signals can be used for visualising the track of the cable [37].

6. References

1. Veselago V.G. “The electrodynamics of substances with simultaneously negative values of ε and μ” Sov. Phys. Usp. 10, 509-514 (1968)
2. Pendry J.B., Holden A.J., Robbins D.J., Stewart W.J. “Magnetism from conductors and enhanced nonlinear phenomena” IEEE Trans. Micr. Theor. Tech. MTT 47, 2075-2084 (1999)
3. Smith D. R., Padilla W.J., Vier D.C., Nemat-Nasser S.C., Schultz S. “Composite medium with simultaneously negative permeability and permittivity” Phys. Rev. Lett. 84, 4184-4187 (2000)
4. Brillouin L. “Wave propagation in periodic structures: electric filters and crystal lattices” 2nd Edn., Dover Publications Inc., New York (1953)
5. Silin R.A., Sazonov V.P. “Slow wave structures” Boston SPA Eng. National Lending Library for Science and Technology (1971)
6. Caloz C., Itoh T. “Electromagnetic metamaterials: Transmission line theory and microwave applications” Wiley Interscience, Hoboken, NJ (2006)
7. Engheta N., Ziolkowski R.W. “Metamaterials” John Wiley and Sons, New York (2006)
8. Solymar L., Shamonina E. “Waves in metamaterials” Oxford University Press, Oxford (2009)
9. Shamonina E., Kalinin V.A., Ringhofer K.H., Solymar L. “Magneto-inductive waveguide” Elect. Lett. 38, 371-373 (2002)
10. Maslovski S., Ikonen P., Kolmakov I., Tretyakov S. “Artificial magnetic materials

based on the new magnetic particle: metasolenoid" PIER 54, 61-81 (2005)

11. Jylhä L., Maslovski S., Tretyakov "Traveling waves along the metasolenoid" Progress in Electromagnetics Research Symposium, Cambridge, MA, March 26-29 (2009)
12. Wiltshire M.C.K., Shamonina E., Young I.R., Solymar L. "Dispersion characteristics of magneto-inductive waves: comparison between theory and experiment" Elect. Lett. 39, 215-217 (2003)
13. Shamonina E., Solymar L. "Magneto-inductive waves supported by metamaterial elements: components for a one-dimensional waveguide" J. Phys. D. 37, 362-367 (2004)
14. Syms R.R.A, Young I.R., Solymar L. "Low-loss magneto-inductive waveguides" J. Phys. D. Appl. Phys. 39, 3945-3951 (2006)
15. Syms R.R.A., Sydoruk O., Shamonina E., Solymar L. "Higher order interactions in magneto-inductive waveguides" Metamaterials 1, 44-51 (2007)
16. Shamonina E., Kalinin V.A., Ringhofer K.H., Solymar L. "Magnetoinductive waves in one, two and three dimensions" J. Appl. Phys. 92, 6252-6261 (2002)
17. Syms R.R.A., Shamonina E., Solymar L. "Positive and negative refraction of magnetoinductive waves in two dimensions" Eur. Phys. J. B 46, 301-308 (2005)
18. Wiltshire M.C.K., Shamonina E., Young I.R., Solymar L. "Resonant magnetic concentrator" Progress in Electromagnetics Research Symposium, October 13-16, Honolulu, Hawaii, USA (2003)
19. Freire M.J., Marques R., Medina F., Laso M.A.G., Martin F. "Planar magneto-inductive wave transducers: Theory and applications" Appl. Phys. Letts. 85, 4439-4441 (2004)

20. Nefedov I.S., Tretyakov S.A. “On potential applications of metamaterials for the design of broadband phase shifters” Micr. Opt. Tech. Letts 145, 98-102 (2005)
21. Syms R.R.A., Shamonina E., Solymar L. “Magneto-inductive waveguide devices” IEE Proc. Micr. Antennas Propag. 153, 111-121 (2006)
22. Freire M.J., Marques R. “Planar magnetoinductive lens for three-dimensional subwavelength imaging” Appl. Phys. Letts. 86, art. 182505 (2005)
23. Sydoruk O., Shamonin M., Radkovskaya A., Zhuromskyy O., Shamonona E., Trautner R., Stevens C.J., Faulkner G., Edwards D.J., Solymar L. “Mechanism of subwavelength imaging with bilayered magnetic metamaterials: theory and experiment” J. Appl. Phys. 101, 073903 (2007)
24. Syms R.R.A., Solymar L., Young M.R. “MR-safe cables – an application of magneto-inductive waves?” Proc. 3rd Int. Cong. on Advanced Electromagnetic Materials in Microwaves and Optics, London, UK, Aug 30–Sept. 4, pp 221-223 (2009)
25. Syms R.R.A., Solymar L., Young I.R. “Periodic analysis of MR-safe transmission lines” IEEE J. Sel. Top. in Quant. Elect., to be published
26. Weiss S., Vernickel P., Schaeffter T., Schulz V., Gleich B. “Transmission line for improved RF safety of interventional devices” Mag. Res. Med. 54, 182-189 (2005)
27. Konings M.K., Bartels L.W., Smits H.F.M., Bakker C.J.G. “Heating around intravascular guidewires by resonating RF waves” J. Mag. Res. Imag. 12, 79-95 (2000)
28. Nitz W.R., Oppelt A., Renz W., Manke C., Lenhart M., Link J. “On the heating of linear conductive structures as guidewires and catheters in interventional MRI” J. Mag. Res. Imag. 13, 105-114 (2001)

29. Shelton D., Tharp J., Zummo G., Folks W., Boreman G. “Fabrication of periodic microstructures on flexible polyimide membranes” J. Vac. Sci. Tech. B 25, 1827-1831 (2007)
30. Shelton D.W., Cleary J.W., Ginn J.C., Wadsworth S.L., Peale R.E., Kotter D.K., Boreman G.D. “Gangbuster frequency-selective surface metamaterials in terahertz band” Elect. Lett. 44, 1288 (2008)
31. Awad M., Nagel M., Kurz H. “Negative-index metamaterial with polymer-embedded wire-pair structures at terahertz frequencies” Opt. Lett. 33, 2683-2685 (2008)
32. Tao H., Strikwerda A.C., Fan C., Bingham C.M., Padilla W.J., Zhang X., Averitt R.D. “Terahertz metamaterials on free-standing highly-flexible polyimide substrates” J. Phys. D. Appl. Phys. 41, 232004 (2008)
33. Tao H., Strikwerda A.C., Fan K., Bingham C., Landy N.I., Shrekhamer D., Pilon D., Padilla W.J., Zhang X., Averitt R.D. “Flexible and reconfigurable THz metamaterials” SPIE Proc. 7394, 73940D (2009)
34. Peralta X.G., Wanke M.C., Arrington C.L., Williams J.D., Brener I., Strikwerda A., Averitt R.D., Padilla W.J., Smirnova E., Taylor A.J., O’Hara J.C. “Large-area metamaterials on thin membranes for multilayer and curved applications at terahertz and higher frequencies” Appl. Phys. Lett. 94, 161113 (2009)
35. Miyamaru F., Takeda M.W., Yaima K. “Characterization of terahertz metamaterials fabricated on flexible plastic films: towards fabrication of bulk metamaterials in terahertz region” Appl. Phys. Exp. 2, 042001 (2009)
36. Krafft A., Müller S., Umathum R., Semmler W., Bock M. “B_1 field-insensitive transformers for RF-safe transmission lines” Mag. Res. Mater. Phys. 19, 257-266

(2006)

37. Burl M. Coutts G.A.Herlihy D., Hill-Cottingham R. Eastham J.E., Hajnal J.V., Young I.R.“Twisted-pair RF coil suitable for locating the track of a catheter” Magn. Reson. Med. 41, 636-638 (1999)

7. Tables

I. Layout and equivalent circuit parameters of experimental thin-film magneto-inductive cables.

8. Figures

1. Magneto-inductive waveguide: a) equivalent circuit, b) and c) axial and planar configurations.
2. Thin-film magneto-inductive cable: a) equivalent circuit, b) geometry; c) resonant element.
3. Thin-film magneto-inductive cable: a) layout parameters, b) overall arrangement, c) experimental realisation in copper-clad polyimide.
4. Experimental variation with the inductor loop length D_L of a) the inductance L and the capacitance C, and b) the resonant frequencies f_0 and f_0'
5. Frequency variation of a) S_{21} and b) S_{11} for two-metre lengths of four different thin-film magneto-inductive cables.
6. a) Equivalent circuit of a terminated magneto-inductive waveguide; b) comparison between S-parameter measurements and theory for two different thin-film MI waveguides. Points are experimental data, and lines are theory.
7. a) Variation with resonant frequency f_0' of the Q-factor and the propagation loss; b)

variation with the inductor loop length D_L of the mid-band impedance Z_{0M}.

Design	D_L (mm)	D_C (mm)	L (nH)	C (pF)	f_0 (MHz)	f_0' (MHz)	Q	κ
A	60.0	20.0	178.4	36.4	62.5	55.5	36.0	0.615
B	65.0	17.5	186.1	30.3	67.0	57.5	36.5	0.625
C	70.0	15.0	196.2	26.3	70.3	61.0	38.0	0.635
D	75.0	12.5	206.8	21.2	76.0	65.0	39.5	0.645
E	80.0	10.0	217.8	17.4	81.8	70.5	41.5	0.655
F	85.0	7.5	229.7	13.0	92.0	79.5	44.0	0.665
G	90.0	5.0	240.9	9.6	104.5	95.0	48.0	0.675
H	95.0	2.5	249.5	6.0	130.0	130.0	55.0	0.690

Table I.

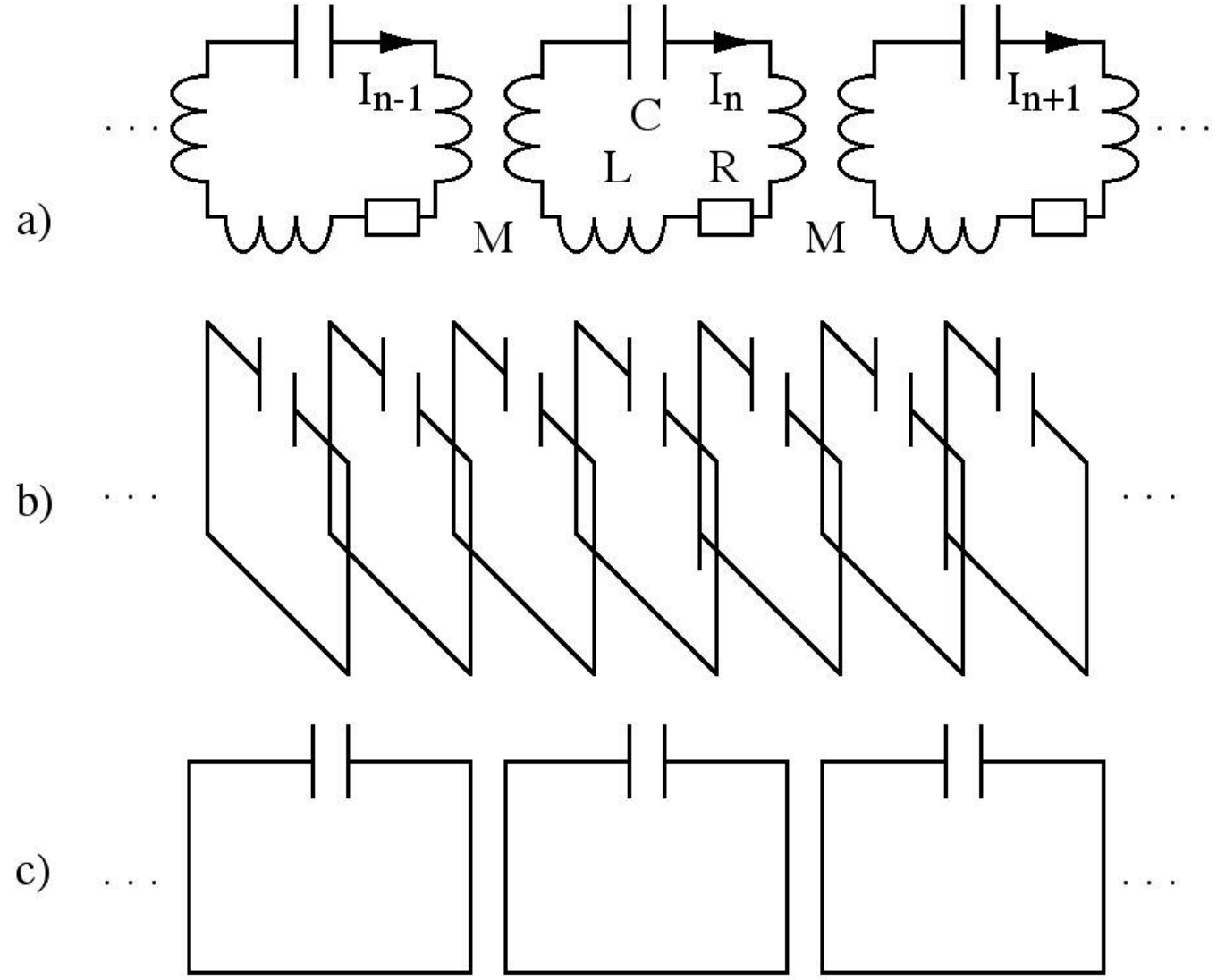

Figure 1a,b,c (Fig1abc.jpg)

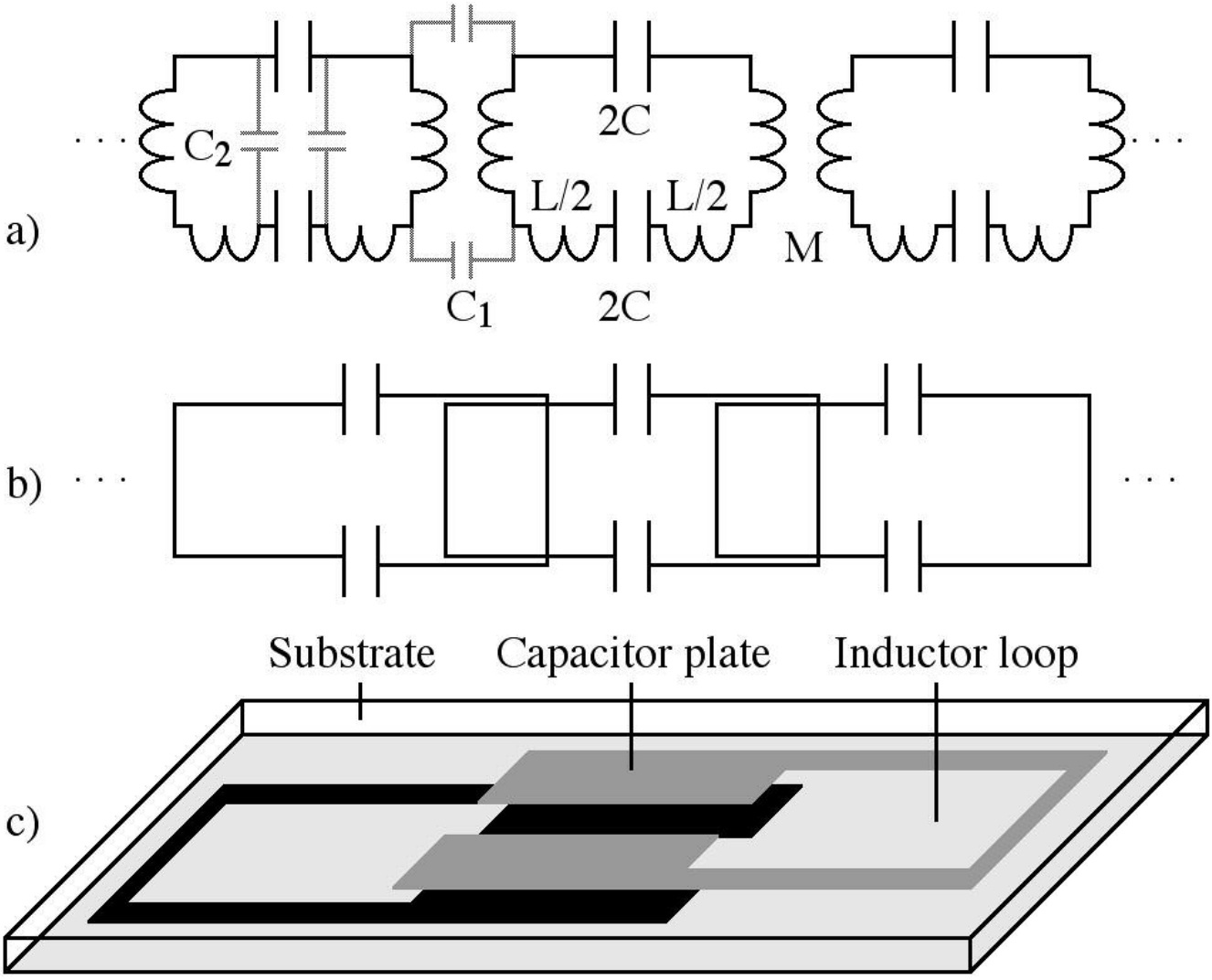

Figure 2a,b,c (Fig2abc.jpg)

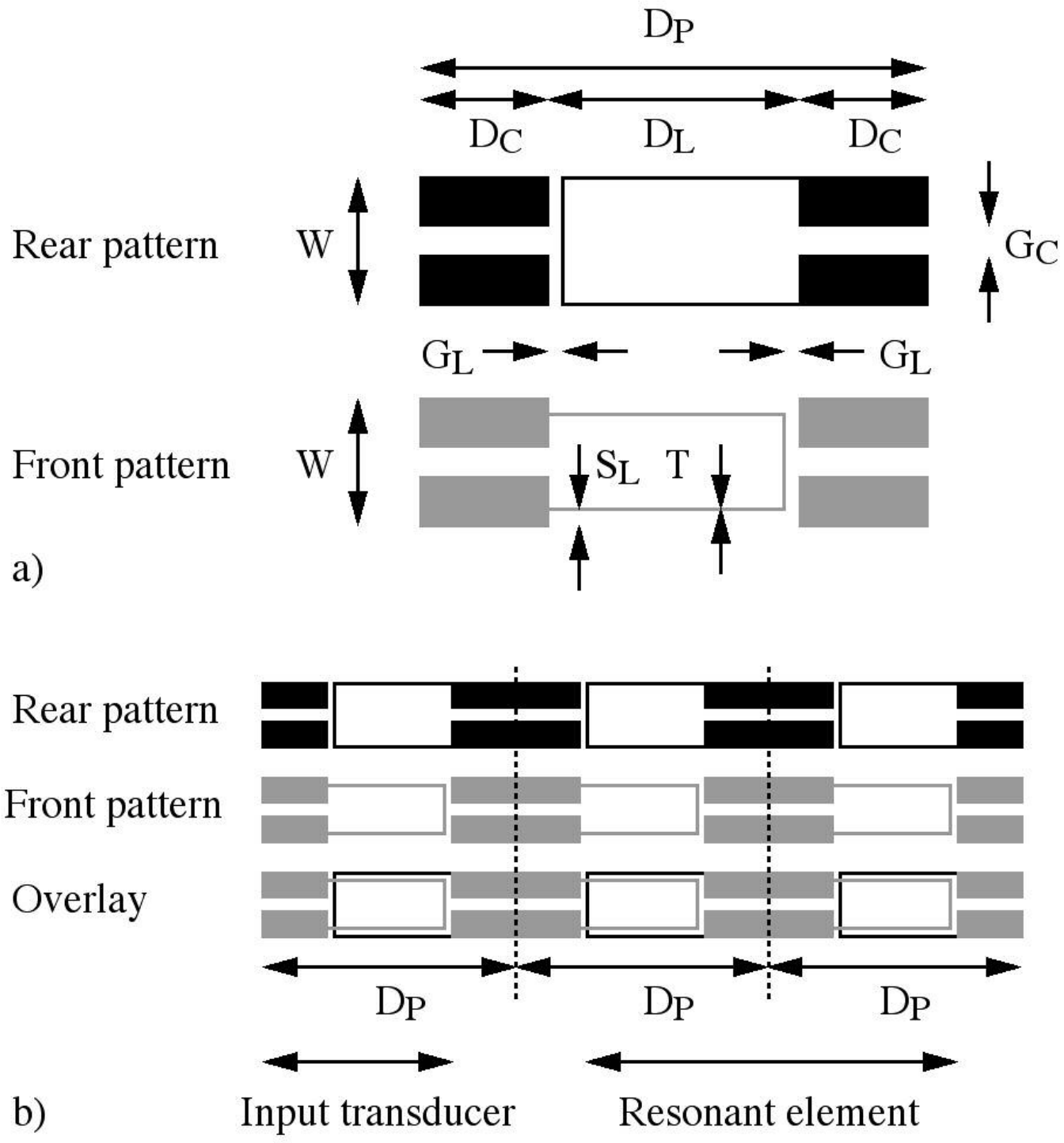

Figure 3a,b (Fig3ab.jpg)

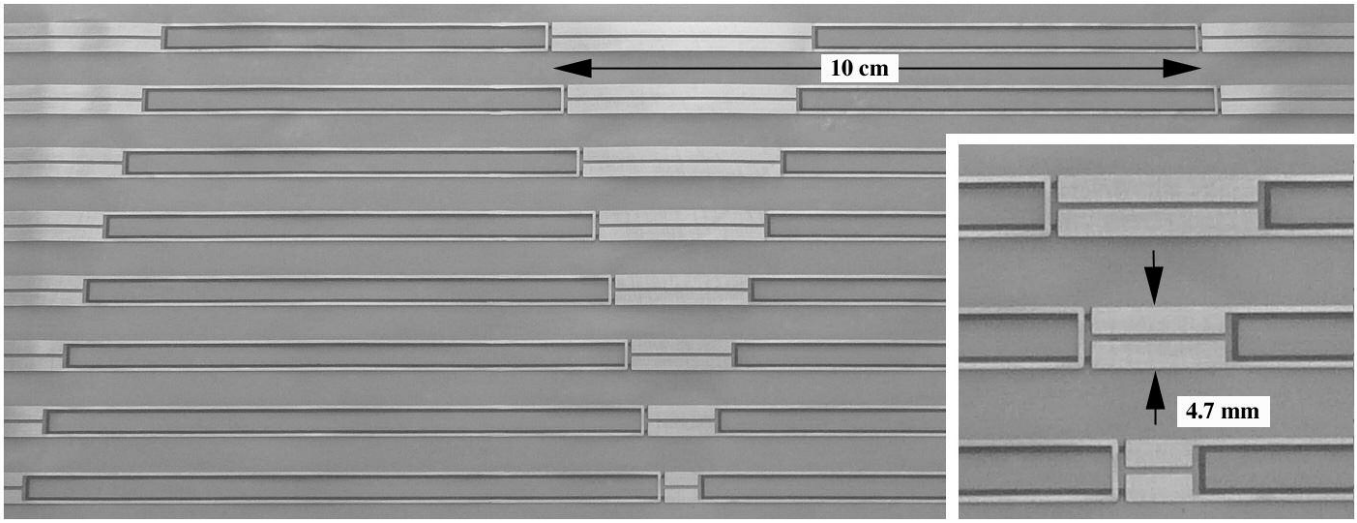

Figure 3c (Fig3c.JPG)

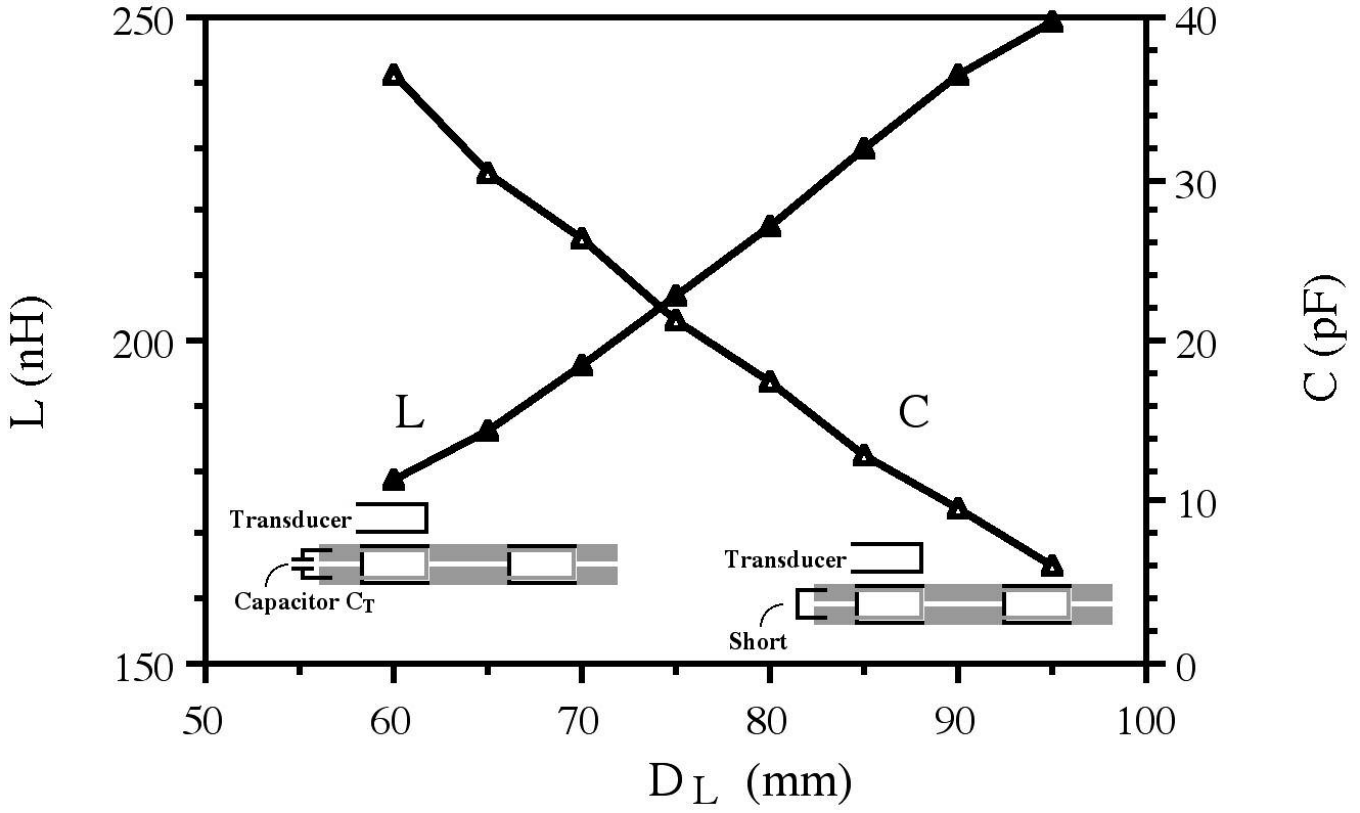

Figure 4a (Fig4a.jpg)

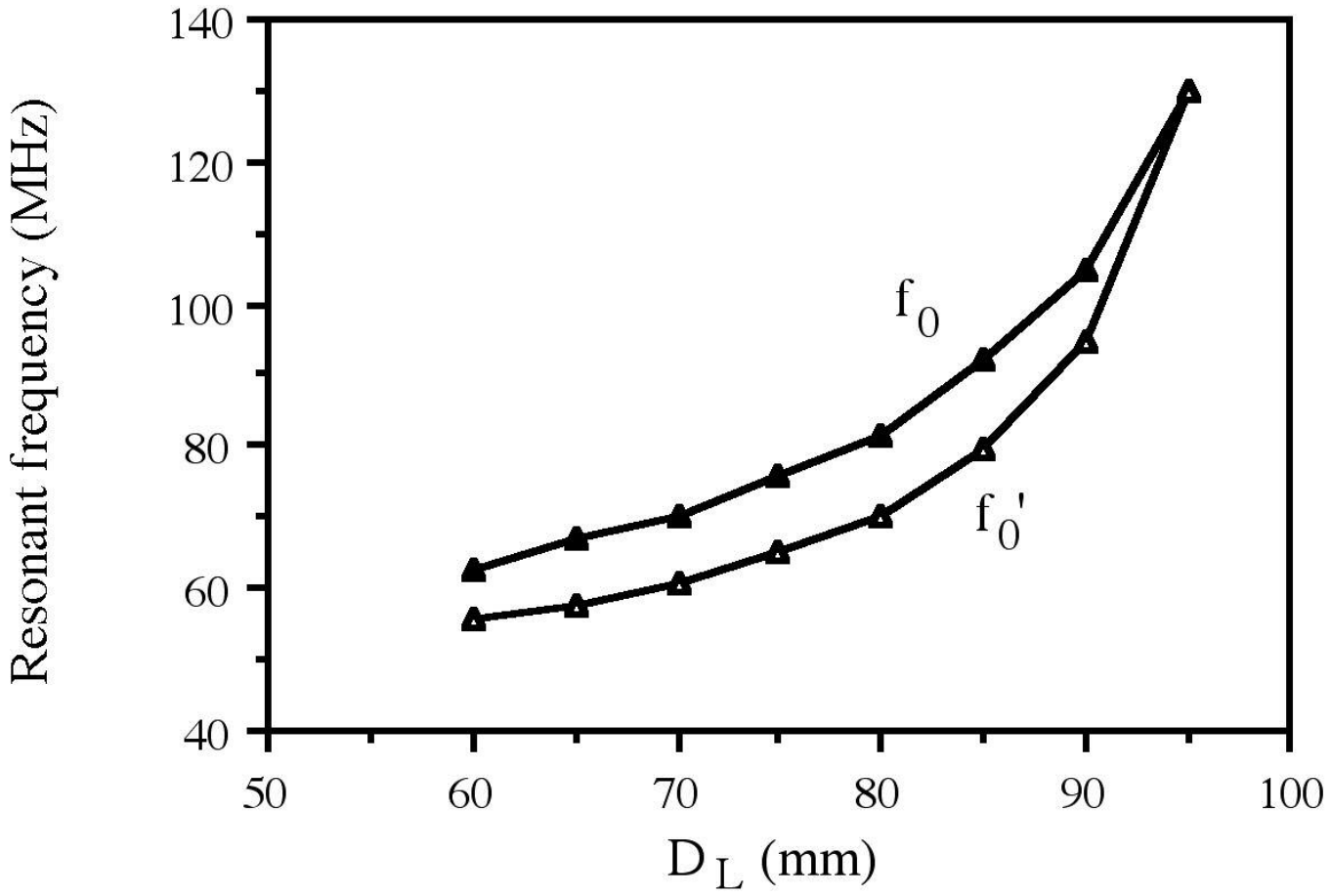

Figure 4b (Fig4b.jpg)

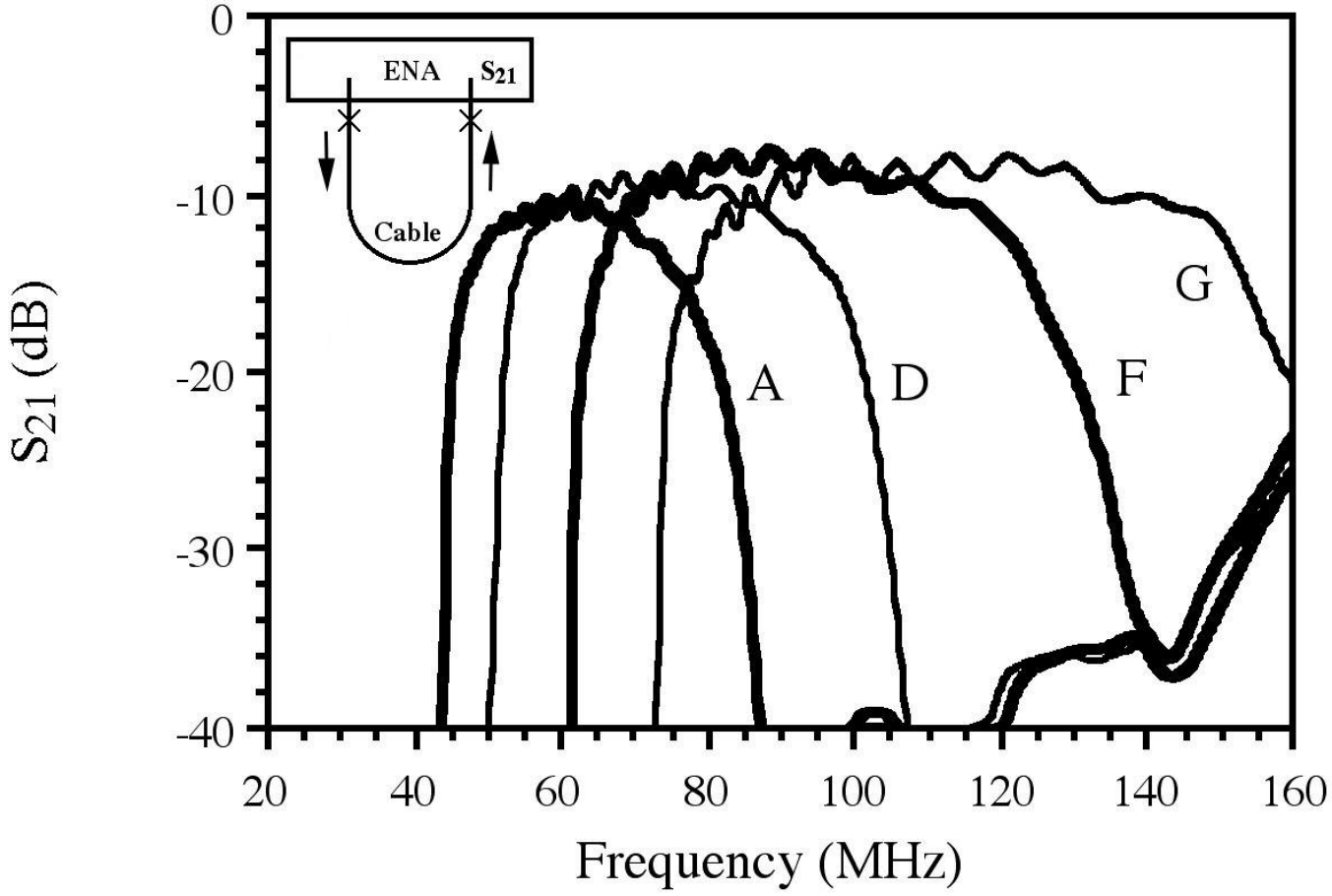

Figure 5a (Fig5a.jpg)

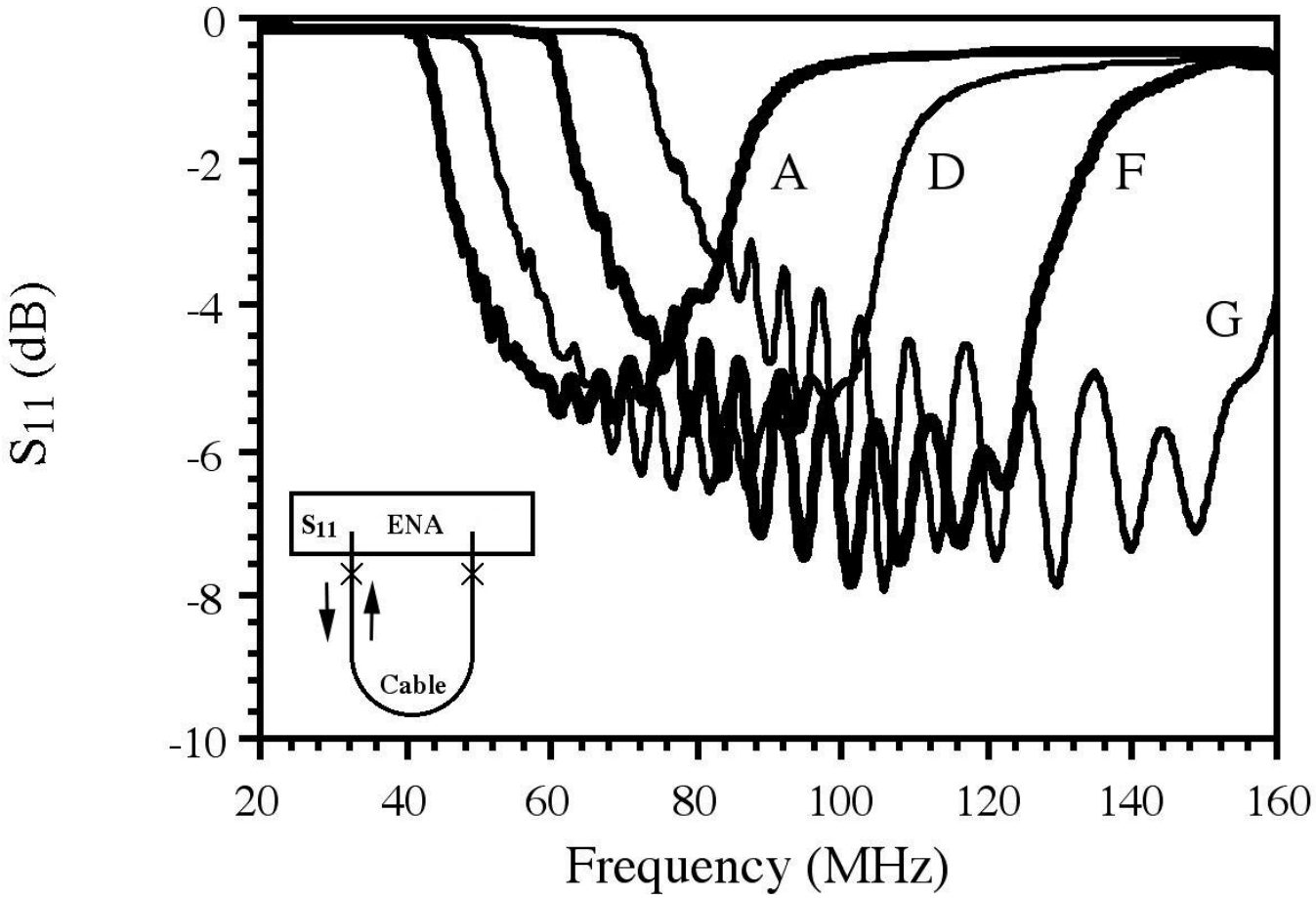

Figure 5b (Fig5b.jpg)

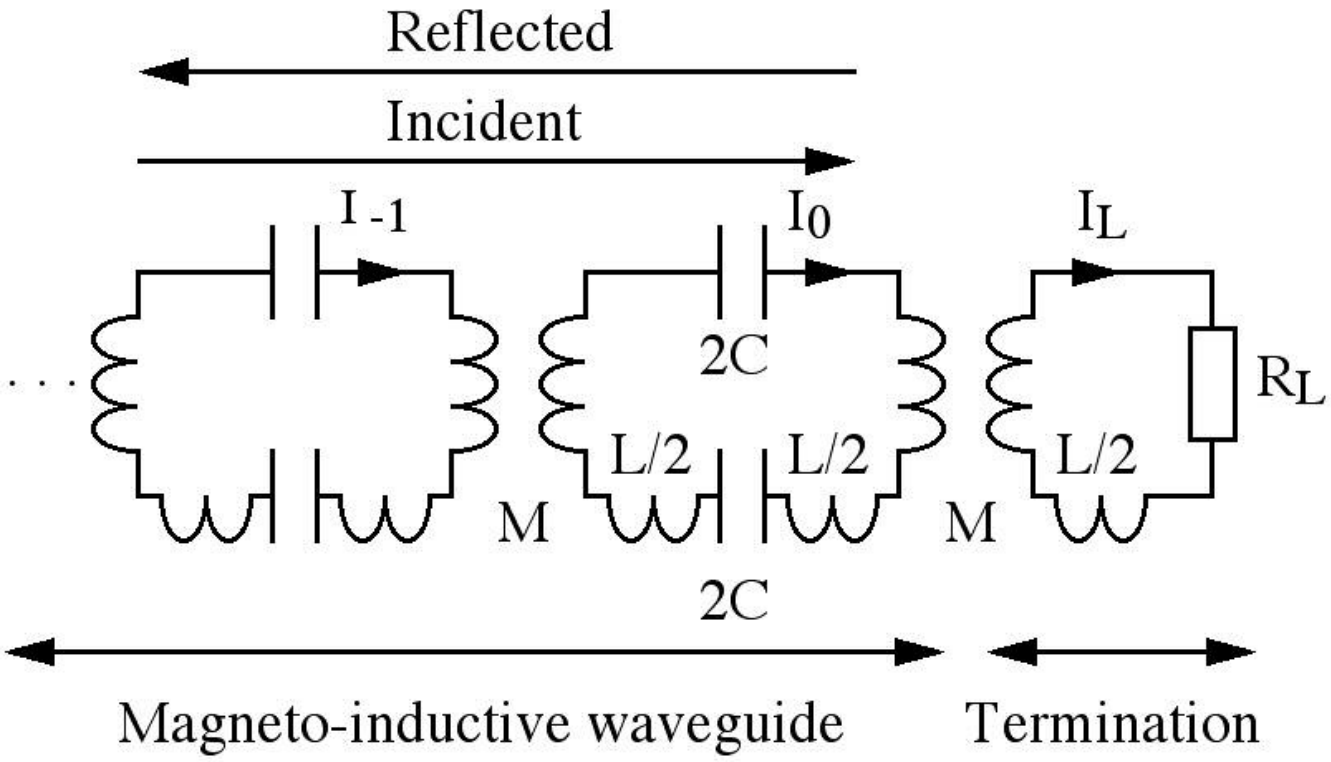

Figure 6a (Fig6a.jpg)

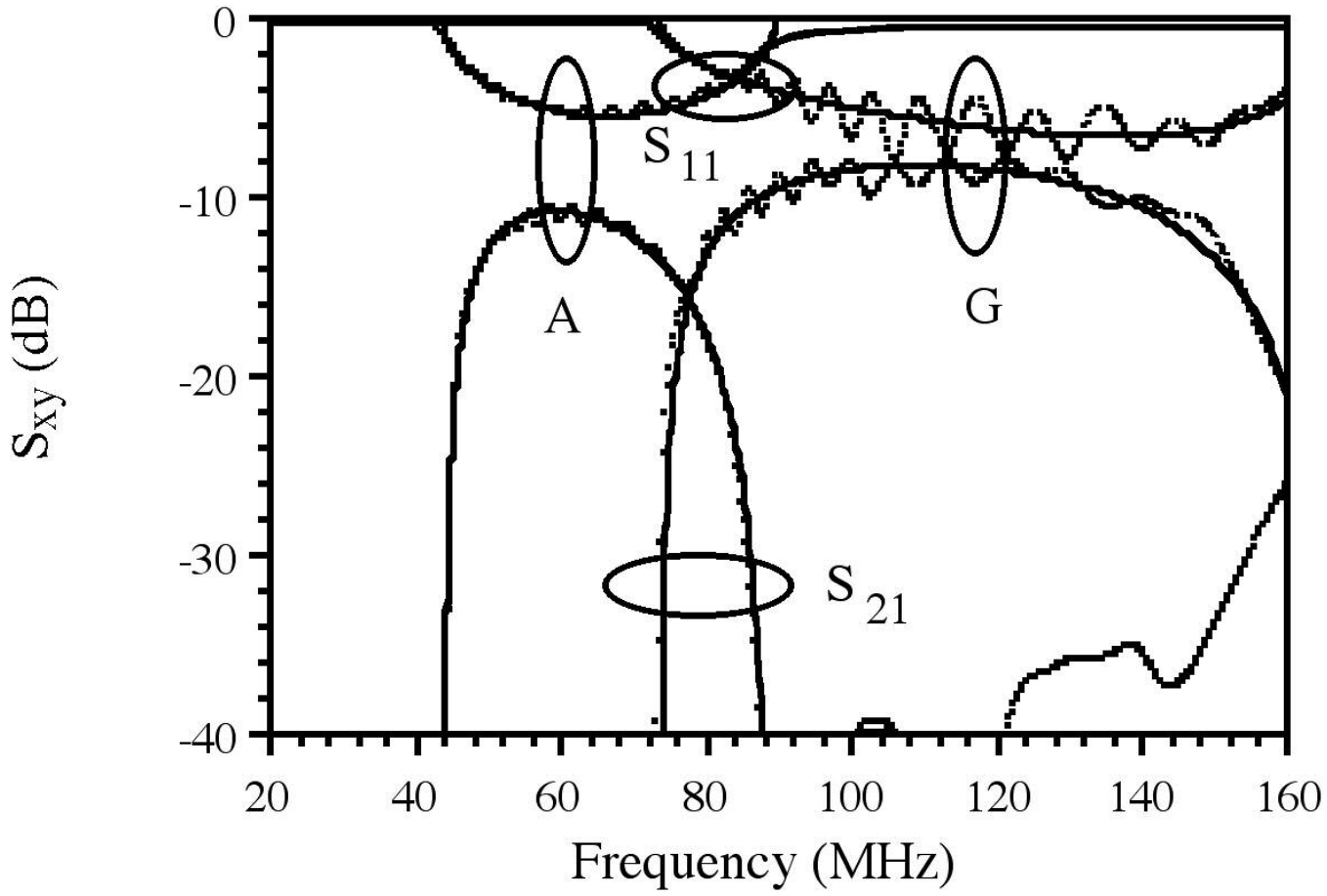

Figure 6b (Fig6b.jpg)

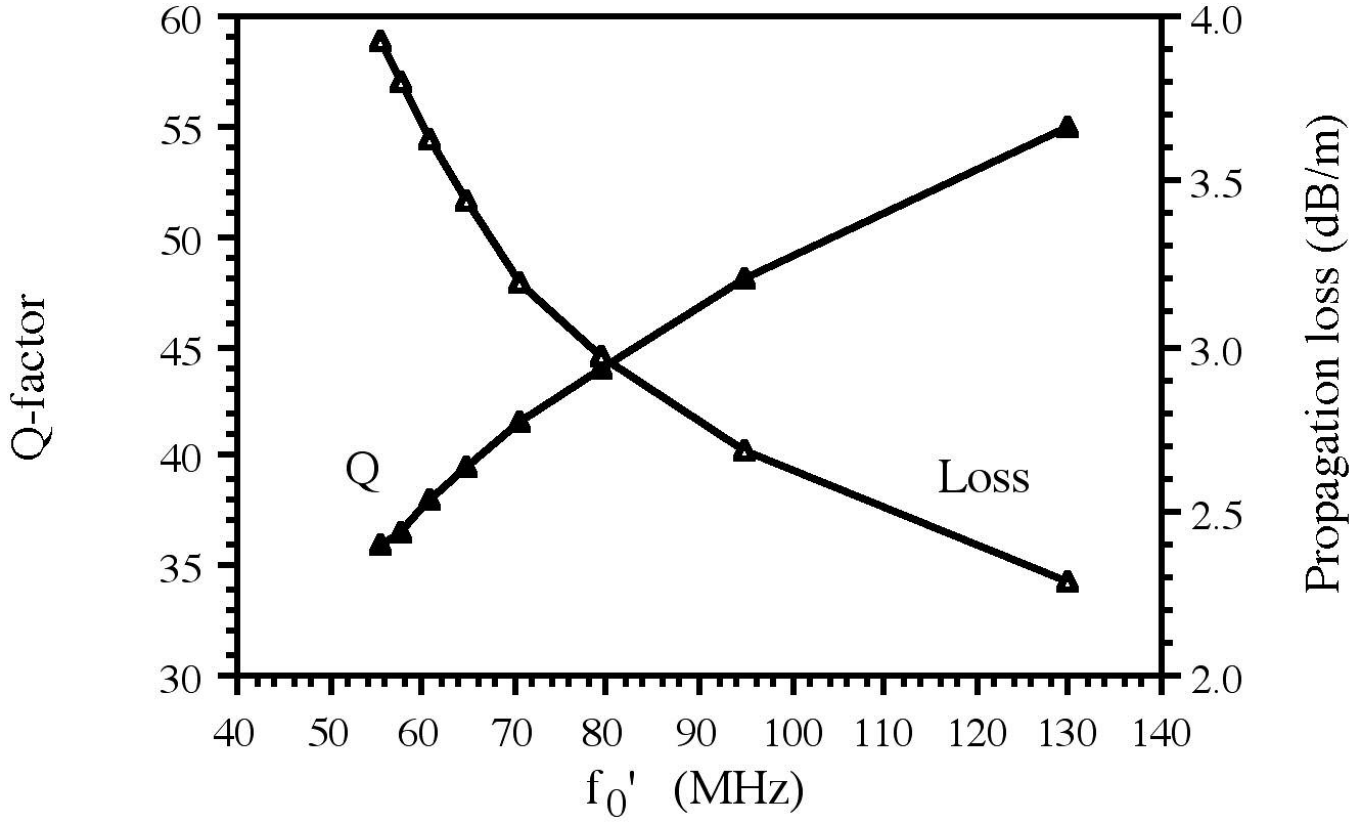

Figure 7a (Fig7a.jpg)

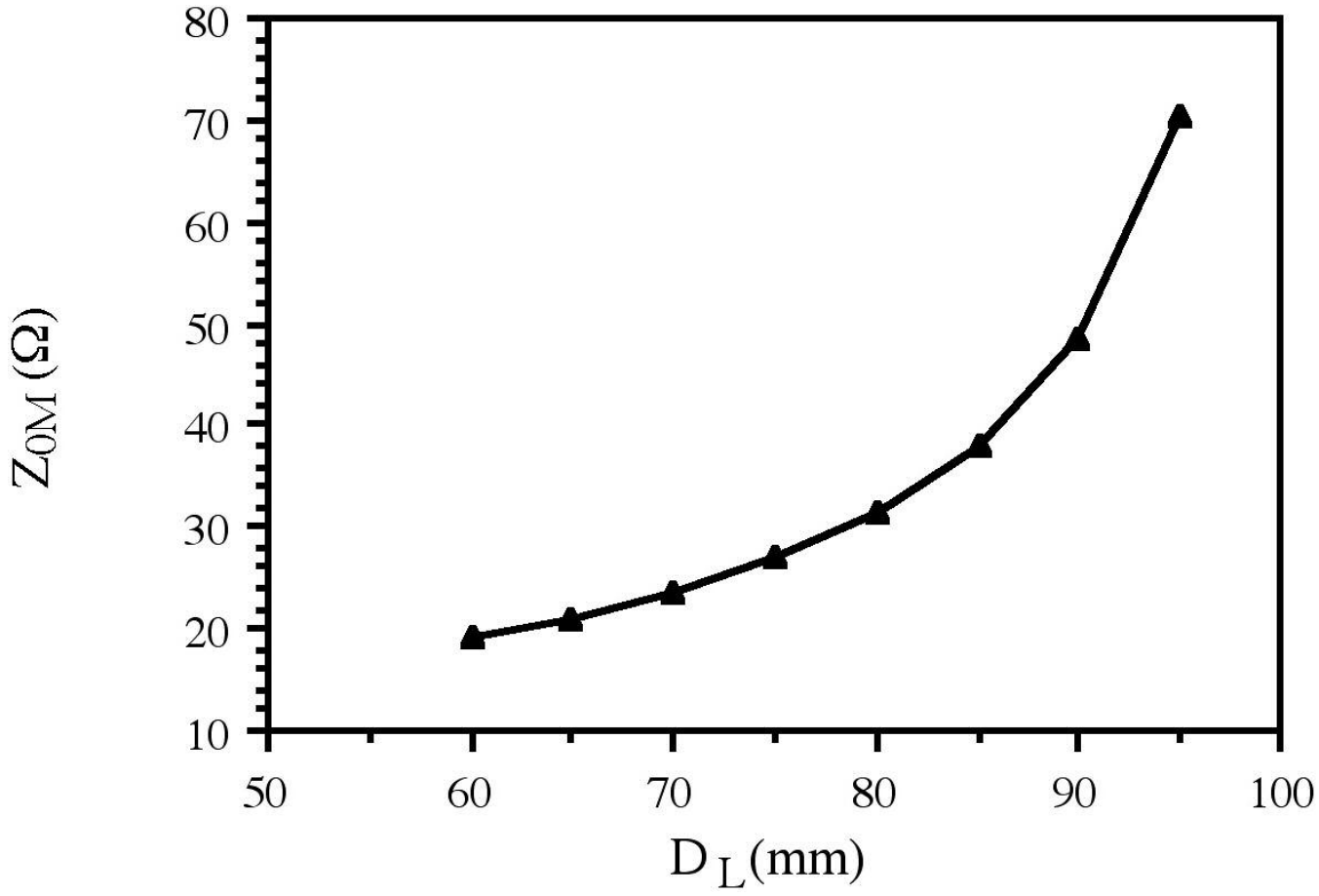

Figure 7b (Fig7b.jpg)